

Imbibition Characteristics and Influencing Factors of the Fracturing Fluid in a Tight Sandstone Reservoir

Tian Li,* Dazhong Ren, Haipeng Sun, Hu Wang, Tao Tian, Qihui Li, and Zhen Yan

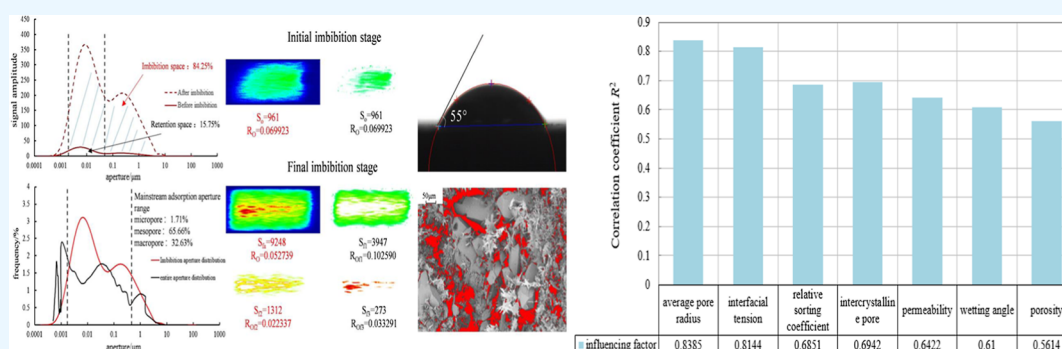
Cite This: *ACS Omega* 2024, 9, 17204–17216

Read Online

ACCESS |

Metrics & More

Article Recommendations



ABSTRACT: The strong reservoir heterogeneity and complex microscopic pore structure in the Linxing area make it prone to water block damage during imbibition development. In order to explore the influence of reservoir microscopic characteristics on imbibition efficiency, taking the tight sandstone gas reservoir in the Linxing area of Ordos Basin as an example, the heterogeneity of the tight sandstone reservoir in the study area is characterized in terms of physical and chemical characteristics as well as the microscopic pore structure. Using nuclear magnetic resonance, high-pressure mercury pressure, and other testing methods, spontaneous seepage experiments in real sandstone were carried out to study the distribution law of different pore structures and seepage characteristics at different times and to systematically evaluate the microscopic pore characteristics of dense sandstone reservoirs and the factors affecting seepage and suction. The results show that due to the strong microscopic heterogeneity of tight sandstone, the macroscopic properties cannot directly reflect the microscopic characteristics, and the response to imbibition efficiency is stronger. The pore size is the main controlling factor affecting imbibition, and the contribution rate of the micropore and mesopore mainstream pore size spaces is higher than that of the macropore. Micropores provide imbibition power, and mesopores provide an imbibition interval. High-porosity and high permeability reservoirs are more conducive to imbibition replacement. The intercrystalline pores have a great influence on the imbibition efficiency, and the influence of intergranular pores and dissolution pores on the imbibition cannot be underestimated. The smaller the relative sorting coefficient, interfacial tension, and contact angle, the better the imbibition effect of fracturing fluid. Research results have theoretical guiding significance for spontaneous imbibition to improve oil recovery.

1. INTRODUCTION

Unconventional oil and gas resources have become an important oil and gas replacement in China, and their development technology is in a stage of rapid development. However, due to the complex nature of such reservoirs, the development methods in different regions are quite different.^{1,2} In order to improve the recovery rate of unconventional oil and gas resources and ensure the efficient utilization of oil and gas resources in China, the development modes of fracture network fracturing and imbibition replacement are often used to develop reservoirs by using capillary force as imbibition power.^{3,4} However, for gravity flow sedimentary tight sandstone reservoirs with strong heterogeneity, there is a lack of explanation for the high retention rate and high production of

fracturing fluid. Especially for tight sandstone gas reservoirs, a large amount of fracturing fluid entering the formation may lead to a serious water lock effect, which makes it difficult for gas reservoirs to break through capillary plugging, thus affecting recovery. Therefore, it is one of the main problems concerning gas field development researchers to clarify the related properties of fracturing fluid, clarify the microscopic

Received: December 17, 2023

Revised: March 11, 2024

Accepted: March 12, 2024

Published: April 4, 2024



Table 1. Basic Parameters of Rock Samples

layer	number	length/cm	diameter/cm	permeability/ $10^{-3} \mu\text{m}^2$	porosity/%
He 8	H1	4.36	3.09	0.308	11.4
	H2	4.47	3.07	0.178	9.3
	H3	4.35	3.05	0.048	5.8
	H4	4.49	3.07	0.013	6.2
	H5	4.53	3.06	0.541	13.2
	H6	4.45	3.05	0.122	9.7

characteristics of reservoirs, and clarify the coupling relationship between fracturing fluid imbibition and reservoir characteristics.

In recent years, more and more scholars have begun to pay attention to the imbibition characteristics and influencing factors of fracturing fluid in tight sandstone reservoirs. These factors include not only the physical properties of the reservoir itself, such as porosity, permeability, mineral composition, etc., but also external conditions such as temperature, pressure, fluid properties, etc.^{5,6} The comprehensive effect of these factors determines the flow and absorption behavior of fracturing fluid in tight sandstone, thus affecting the imbibition effect. For example, Liu et al.^{7,8} considered that adsorption thickness and pore throat connectivity are the key factors affecting matrix permeability and spontaneous imbibition displacement efficiency. The difference in the imbibition methods determines the degree of influence of permeability on the imbibition rate. At the same time, it is pointed out that the fracture can significantly increase the contact area between the dense matrix and the imbibition liquid, thereby improving the imbibition recovery. Zhou et al.^{9–12} studied the influence of pore structure and fluid properties on imbibition. The results show that imbibition is affected by many factors, including pore structure, fluid properties, and fracture development degree. Through numerical simulation and accurate acquisition of key seepage parameters, the imbibition process can be predicted, and the gas production process can be optimized. Gao et al.^{13–15} discussed the influence of salinity, temperature, pressure, and other factors on static imbibition. It is believed that under conditions of high salinity, the imbibition effect increases with an increase in temperature or pressure. Bussche et al.^{16–18} analyzed the effect of salinity and salt concentration of fracturing fluid on imbibition displacement and believed that the main reason for osmotic pressure was the difference of salinity. Low salinity water and an appropriate cation concentration could effectively improve the oil recovery effect.

This work focuses on the tight sandstone reservoirs of the Upper Shihezi Formation, specifically the He 8 member in the Linxing area of the Ordos Basin in the Permian System. By employing experimental techniques such as nuclear magnetic resonance (NMR), scanning electron microscopy (SEM), high-pressure mercury intrusion, and gas adsorption, we aim to reveal the microscopic characteristics of tight sandstone reservoirs. Additionally, through imbibition experiments, we analyze the impact of these microscopic features on the imbibition efficiency of fracturing fluids. Our research not only achieves a comprehensive characterization of the reservoir in terms of multiple parameters and scales but also elucidates various factors influencing imbibition efficiency and their governing patterns. These findings hold crucial guidance for enhancing fracturing technologies and increasing the recovery rates of unconventional oil and gas resources. Furthermore, the insights gained provide a theoretical foundation for alleviating

and preventing water blocking damage and improving the effectiveness of imbibition-driven oil recovery processes.

2. EXPERIMENTAL SAMPLES AND METHODS

2.1. Experimental Samples. 2.1.1. Experimental Core.

The samples for this study are derived from the eighth member of the He 8 member of the Linxing block in the Ordos Basin. The four sides of the basin are controlled by the Yinshan fold, the Qinling orogenic belt, the Ordos platform margin fold belt, and the western Shanxi flexural fold belt. The overall display is deep in the west and low in the east, deep in the south, and low in the north.^{19,20} The stratigraphic depth is 3200–3500 m, and the contact relationship between the upper and lower strata is parallel unconformity. According to the principle of representative characteristics on the plane and vertical plane, six rock samples at different depths were selected and labeled to carry out basic physical property test experiments. The basic parameters of the samples are listed in Table 1. The porosity of rock samples is between 5.8 and 13.2%, with an average of 10.2%, and the permeability is between 0.013×10^{-3} and $0.541 \times 10^{-3} \mu\text{m}^2$, with an average of $0.202 \times 10^{-3} \mu\text{m}^2$.

2.1.2. Experimental Fluid. According to the fracturing fluid formula obtained from the field practice in the study area, combined with the cleanup agent (adding 0.3% cleanup agent) and waterproof lock agent (adding 0.1% waterproof lock agent), the experimental fracturing fluid is configured.

2.2. Experimental Method. 2.2.1. Pressurized Mercury.

The PoreMaster 33 high-pressure mercury porosimeter was used. The aperture distribution was measured in the range of 0.0036–1000 μm . The mercury injection capillary pressure can be continuously or step-by-step pressurized from a vacuum to 200 MPa. The experimental rock samples were placed in a constant temperature box (temperature 75 °C, time 12 h), dried, and then cooled to room temperature. According to the method (GB/T 21650.1–2008),²¹ the pore distribution, pore volume, pore surface area, and other parameters were determined.

2.2.2.2. Nuclear magnetic resonance. A mesoMR23–60H–I low-field NMR analyzer was used, and the CPMG sequence was used as the standard sequence for T_2 determination. The resonance frequency of the instrument is 2.38 MHz, the magnetic field intensity is 0.54 T, the number of echoes is 2048, the scan times (NS) are 32 ms, the echo time (TE) is 0.6 ms, and the ambient temperature is controlled at 22 ± 0.5 °C to ensure the accuracy and reliability of the experimental results. NMR tests were carried out on cores with saturated fracturing fluid at different imbibition times, and the volume of fracturing fluid in core pores was calculated according to the T_2 amplitude obtained.²² The imbibition efficiency of fracturing fluid in core pores during spontaneous imbibition was calculated by T_2 signal values at different relaxation times.²³

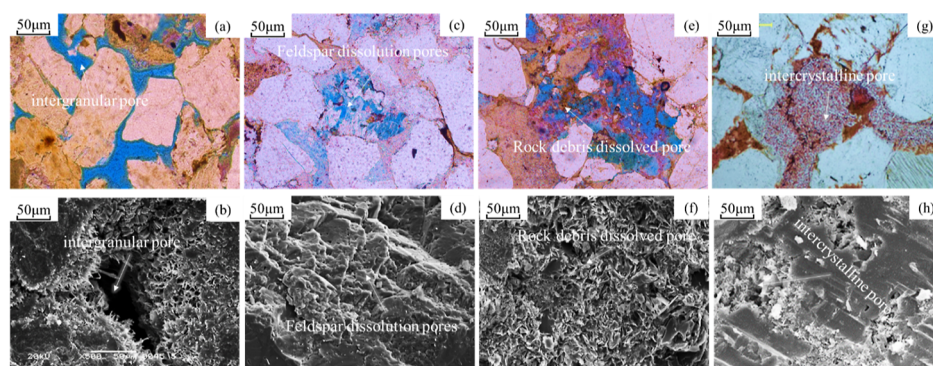


Figure 1. Petrographic thin sections of clastic components in the study area (a) intergranular pore, magnification 2000 \times , depth 1864.66 m; (b) intergranular pore, magnification 100 \times , depth 1823.12 m; (c) feldspar dissolution pores, magnification 2000 \times , depth 1872.56 m; (d) feldspar dissolution pores, magnification 200 \times , depth 1982.26 m; (e) rock debris dissolved pore, magnification 2000 \times , depth 1841.75 m; (f) rock debris dissolved pore, magnification 100 \times , depth 1611.75 m; (g) intercrystalline pore, magnification 2000 \times , depth 1881.35 m; and (h) intercrystalline pore, magnification 100 \times , depth 1847.17 m.

Table 2. Statistical Table of Different Types of Face Rates

layer		intergranular pore/%	feldspar dissolution pores/%	rock debris-dissolved pore/%	intercrystalline pore/%	microfissure/%	surface pore rate/%
He 8	Min-value	0.2	1.5	1.6	0.4	0.0	2.62
	Max-value	3.5	6.1	6.9	1.4	0.7	9.55
	Mean-value	2.4	4.5	4.9	1.1	0.6	5.12

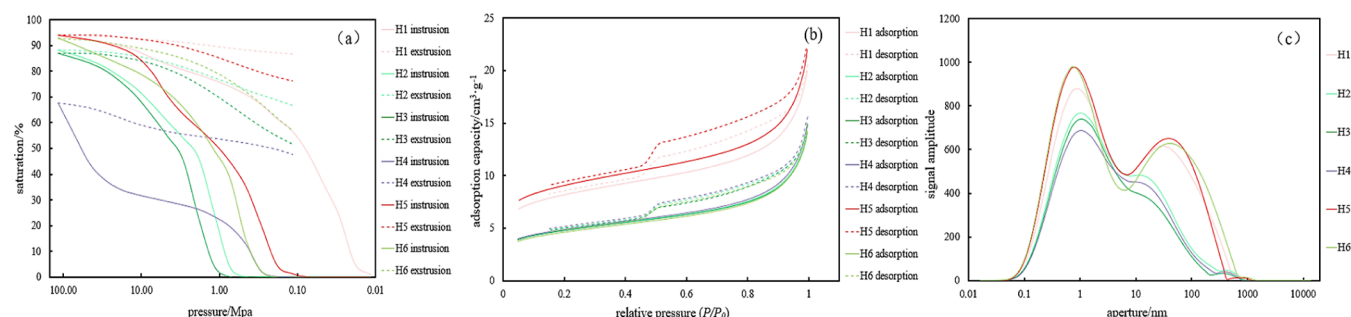


Figure 2. Analysis of different experimental methods (a) Mercury injection, (b) Nitrogen adsorption, and (c) Nuclear magnetic T_2 .

2.2.3. Gas Adsorption. The pore parameters of the samples were determined by a TriStar II 3020 automatic specific surface and pore analyzer. The specific surface area measured by the instrument is less than 0.0005 m²/g, and the lower limit of pore volume is less than 0.0001 cm³/g. According to the method of (GB/T 21650.2–2008),²⁴ 2–5 g of the sample was crushed to 40–60 mesh and vacuum-dried at 100 °C for 12 h, and the moisture and volatile gas in the rock sample were removed. The instrument was vacuumized at 200 °C for 4 h and injected with nitrogen or carbon dioxide gas for experimental testing.

2.2.4. Imbibition.

- (1) The core was washed with oil and dried in a 70 °C incubator until the sample quality did not change significantly, and the dry weight and size were measured.
- (2) The dried core is lifted with a fish line and immersed in a beaker filled with fracturing fluid to ensure that the core is located below the solution level and placed vertically; that is, the core is completely immersed in the fracturing fluid.
- (3) In the process of core imbibition, according to the laboratory measurement specification of NMR parameters of rock samples,²⁵ the NMR experiments were used

to monitor rock samples at different imbibition stages, and pseudocolor imaging tests were carried out.

- (4) The tested core was reimmersed in the fracturing fluid, and step (2) (3) was repeated to continue the imbibition experiment.

3. RESULTS

3.1. Pore Structure Characterization. 3.1.1. Pore Type.

Different pore types reflect the differences of reservoir diagenesis type and reservoir pore throat complexity.²⁶ Through the microscopic analysis of a large number of casting thin sections and SEM, it was found that the study area showed a variety of pore types (Figure 1). Due to the later strong compaction, diagenesis, and cementation, the primary pores in the deep layer of the He 8 section are obviously reduced, and the secondary pores formed by the later dissolution and relatively few fractures constitute the main pore types of the reservoir. In general, the pore types include intergranular pores, dissolved pores, and intercrystalline pores, and the cracks are mainly microcracks; the matrix pores are mainly intergranular pores, the degree of microfracture development is extremely low, and the fracture trend is random. According to the pore type and surface porosity of the reservoir (Table 2), it

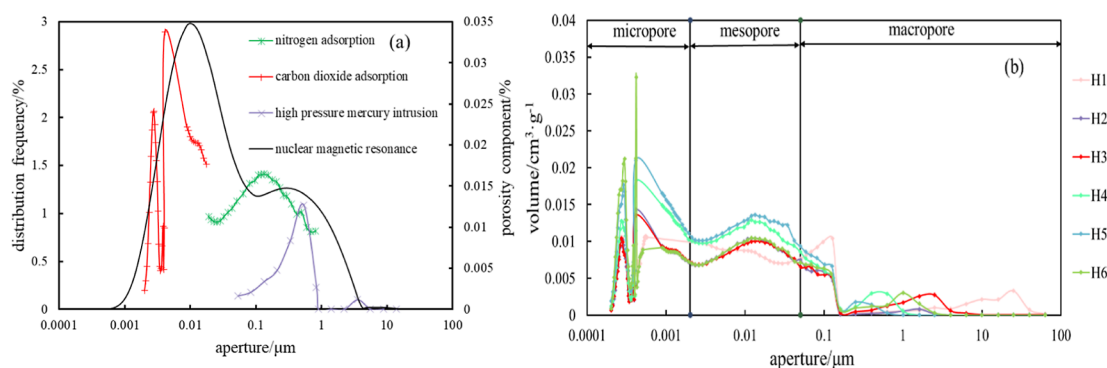


Figure 3. Combined with high-pressure mercury intrusion and gas adsorption to characterize pore-throat distribution characteristics. (a) Analysis and comparison of different methods. (b) Full aperture distribution.

Table 3. Full-Aperture Pore Structure Parameters of Tight Sandstone Rock Samples^a

specimen	aperture ratio (%)			total specific surface area (m ² /g)	stage specific surface area (m ² /g)			total pore volume (cm ³ /g)	stage pore volume (m ³ /g)		
	micropore	mesopore	macropore		S ₀	S ₁	S ₂		V ₀	V ₁	V ₂
H1	53.01	27.42	19.57	743.132 (100%)	679.631 (91.45%)	62.294 (8.38%)	1.207 (0.16%)	0.639 (100%)	0.293 (45.70%)	0.148 (23.16%)	0.198 (31.14%)
H2	49.80	24.19	26.01	747.103 (100%)	677.770 (90.72%)	68.541 (9.17%)	0.789 (0.11%)	0.492 (100%)	0.243 (49.39%)	0.198 (40.24%)	0.051 (10.37%)
H3	47.50	27.16	25.34	715.703 (100%)	655.061 (91.53%)	59.565 (8.32%)	1.077 (0.15%)	0.568 (100%)	0.242 (42.61%)	0.187 (32.92%)	0.139 (24.47%)
H4	48.10	24.18	27.72	983.481 (100%)	901.528 (91.67%)	80.675 (8.20%)	1.278 (0.13%)	0.715 (100%)	0.350 (48.95%)	0.241 (33.71%)	0.124 (17.34%)
H5	53.85	28.75	17.40	1207.623 (100%)	1121.24 (92.85%)	84.935 (7.03%)	1.448 (0.12%)	0.755 (100%)	0.407 (53.91%)	0.259 (34.30%)	0.089 (11.79%)
H6	49.60	27.16	23.24	1217.306 (100%)	1155.569 (94.93%)	60.545 (4.97%)	1.192 (0.10%)	0.794 (100%)	0.472 (59.45%)	0.192 (24.18%)	0.130 (16.37%)

^aS—total specific surface area; S₀—microporous specific surface area; S₁—specific surface area of mesopores; S₂—macroporous specific surface area. V—total pore volume; V₀—pore microscopic volume; V₁—mesoporous pore volume; and V₂—the pore volume of macropores. The number in parentheses is the proportion of various pores to the specific surface area or pore volume.

can be found that the surface porosity of the He 8 reservoir is between 2.62 and 9.55%, with an average of 5.12%.

3.1.2. Aperture Distribution. Carbon dioxide adsorption, low-temperature nitrogen adsorption, and mercury intrusion experiments belong to fluid intrusion experiments.²⁷ The pore-throat distribution and connectivity under different apertures are obtained by using air and mercury intake under different pressure conditions. The main difference between the three experiments is that the experimental principle and pore-throat size range are different. In the mercury injection experiment, since mercury is a nonwetting phase, the capillary force is overcome under the mercury injection pressure to preferentially enter the larger pore-throat space. This method can characterize the micronano pore-throat space in the range of 0.0036–1000 μm. However, due to the limitation of mercury injection pressure, this method cannot be used to characterize the smaller pore-throat space. The mercury injection curve characteristics of the experimental samples (Figure 2a) show high mercury injection pressure and high saturation. With the slow increase of mercury injection pressure, the displacement pressure is low, and the mercury removal efficiency is high, ranging from 7.59 to 40.54%, with an average of 26.65%, indicating that the pore structure of “macropore-fine throat” is mostly developed in the reservoir. Carbon dioxide and nitrogen are preferentially adsorbed on the surface of smaller

pore-throats after entering the pore space, which can characterize the nanoscale pore-throat space in the range of 0.35–200 nm. The nitrogen adsorption curve characteristics of the experimental samples (Figure 2b) have IV (a) adsorption isotherm and H3 type hysteresis loop type characteristics,²⁸ indicating that the pore structure is complex, H1 and H5 hysteresis loops are relatively large, there are more ink bottle-shaped pores, and the porosity is relatively large. The hysteresis loops of samples H2, H3, H4, and H6 are small, there are wedge-shaped pores, and the porosity is small.²⁹ However, this method is based on the capillary condensation of carbon dioxide and nitrogen in the critical state to estimate aperture distribution. The larger the pore-throat is, the greater the pressure required for filling, and the filling pressure cannot exceed the saturated vapor pressure of the gas. Otherwise, a large error will be generated when characterizing the pore-throat distribution, resulting in a decrease in the characterization accuracy of the larger pores. Therefore, the combination of the three experimental methods can more accurately characterize the size and distribution of pore-throats in tight sandstone reservoirs. The NMR experiment itself can monitor the aperture range of 0.2 nm ~200 μm, and high mercury pressure (Figure 2a) and high relative pressure (Figure 2b) correspond to small apertures (Figure 2c). Therefore, the NMR and full aperture methods can be used

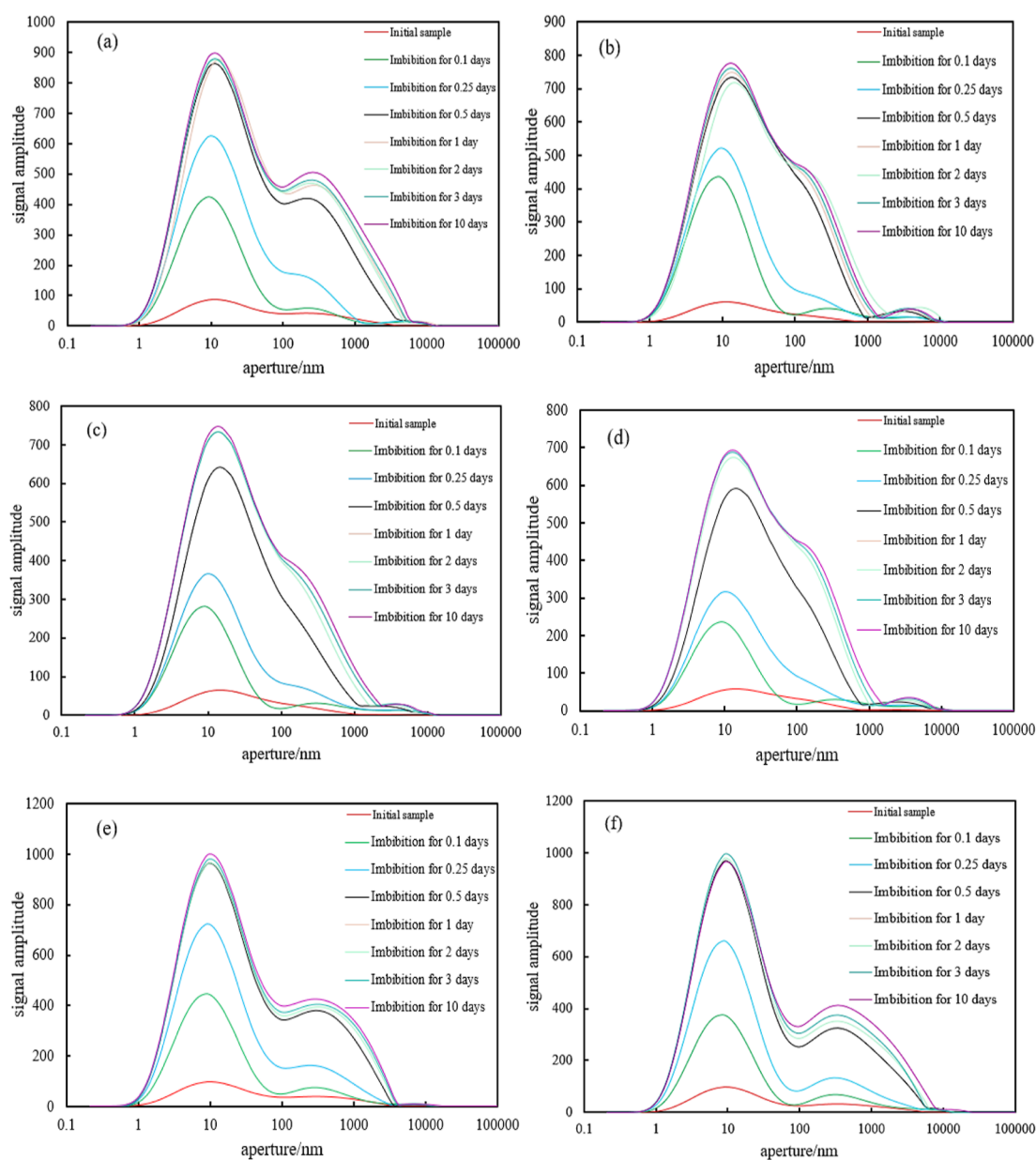


Figure 4. Suction-NMR T_2 spectrum curve. (a) H1 Imbibition T_2 spectrum, (b) H2 Imbibition T_2 spectrum, (c) H3 Imbibition T_2 spectrum, (d) H4 Imbibition T_2 spectrum, (e) H5 Imbibition T_2 spectrum, and (f) H6 Imbibition T_2 spectrum.

to compare (Figure 3a) and monitor the difference.³⁰ According to the analysis of the experimental results, the pore-throat distribution curve obtained by mercury intrusion and nitrogen adsorption tests has a good superposition phenomenon when the pore-throat radius is less than 0.1 μm . Therefore, the part of the pore-throat detected by mercury intrusion and nitrogen adsorption can be spliced together to characterize the pore-throat distribution characteristics of tight sandstone reservoirs so as to obtain the full-scale aperture distribution (Figure 3b) and further study the influence of different apertures on imbibition.

Based on the classification method of pore-throat space of the tight sandstone reservoir in relevant industry standards,³¹ combined with the joint characterization of pore-throat distribution characteristics in the study area, the pore-throat space of the tight sandstone reservoir in the study area is divided into three types of micropores (50 nm) with the pore-

throat radius of 2 and 50 nm as the boundary, and the pore structure parameters can be obtained (Table 3). Based on the comprehensive characterization results of pore volume and pore size (Figure 3b), combined with Table 3, it can be seen that the pore size distribution of tight sandstone reservoirs in the study area ranges from 0.21 nm to 63 μm . The average contents of micropores, mesopores, and macropores were 50.31, 26.48, and 23.21%, respectively. The distribution patterns of pore volume, specific surface area, and pore size are consistent. The average specific surface area accounted for 92.19%, mesopores for 7.68%, and macropores for 0.13%. Micropores dominate the specific surface area, which not only reveals the complexity and diversity of pores on this scale but also indicates good pore connectivity. In terms of pore volume, the average micropore is 48.93%, the mesopore is 26.55%, and the macropore is 24.52%. The maximum increment of pore volume appears at 0.41 and 0.29 nm, indicating that the

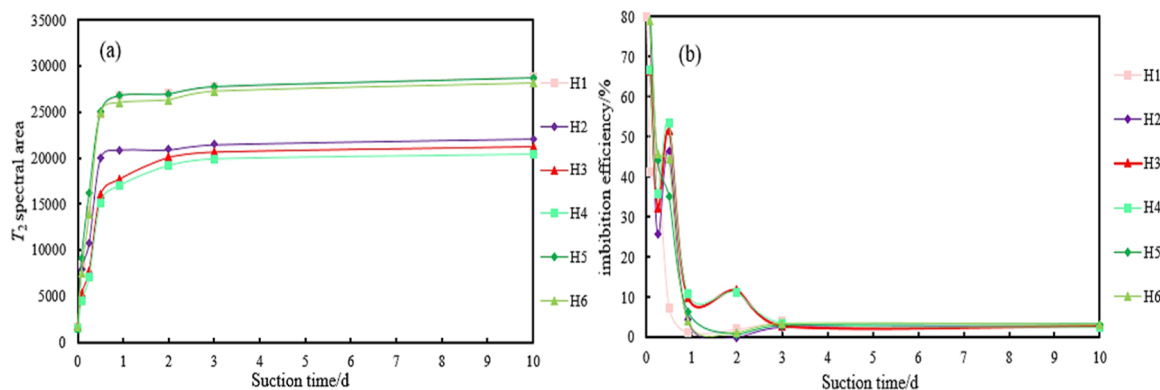


Figure 5. Imbibition T_2 spectra. (a) T_2 spectral area under different imbibition times and (b) variation range of imbibition efficiency.

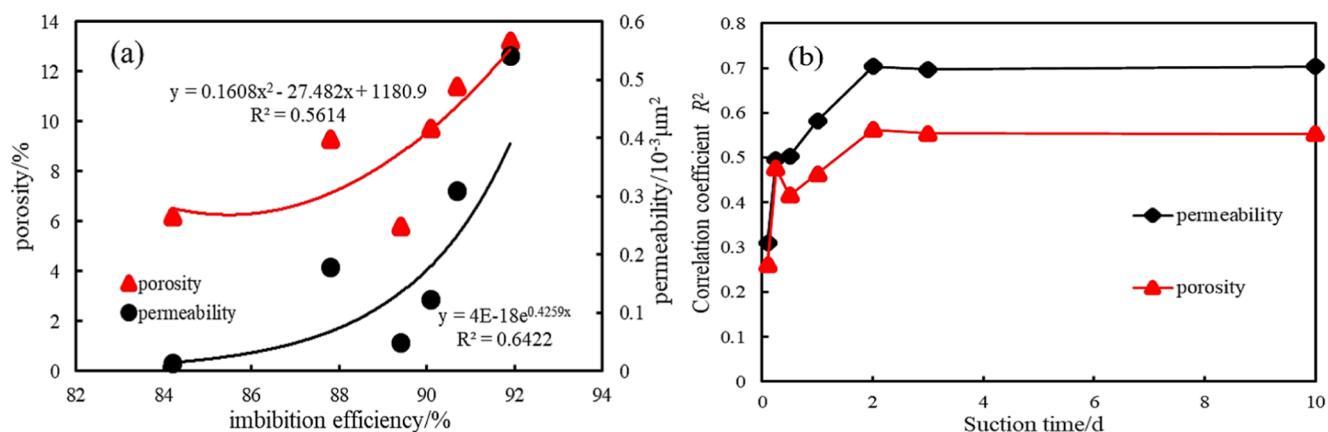


Figure 6. Relationship between physical properties and imbibition efficiency. (a) porosity infiltration and imbibition efficiency and (b) correlation between pore permeability and imbibition efficiency.

abundance of micropores at these diameters is the highest. In general, the main pore distribution in this region is composed of micropores less than 2 nm, of which micropore-specific surface area and pore volume contribute the most. This emphasizes that micropores are the main storage space for the tight sandstone gas in the He 8 member that was studied.

3.2. Imbibition Characteristics of Different Pore Structures. The fracturing fluid imbibition experiment was carried out on the rock samples of the tight sandstone reservoir in the study area, and the water saturation of the rock samples after imbibition was tested by an NMR experiment. The signal amplitude curve corresponding to the NMR T_2 spectrum of core imbibition is shown in Figure 4. Within 0.5 days before imbibition, the amplitude of the T_2 spectrum signal increases obviously. By comparing and analyzing the amplitude and area of the T_2 spectrum signal of 6 cores (Figure 5), it can be found that the amplitude of the H4 signal increases slowly, the area of T_2 is the lowest, and the signal amplitude remains low after imbibition, which indicates that the pore structure is complex and the imbibition efficiency of the fracturing fluid is low. Combining the characteristics of low porosity, low permeability, and a small pore-throat structure of core H4, it shows that the denser the core is, the worse the imbibition degree is.

By comparing the T_2 spectra of different pore structures (Figure 4), it can be found that they are generally bimodal curves. The left peak of the curve represents the signal of smaller pores (micromesopores), and the right peak represents the signal of larger pores (macropores, microfractures). On the whole, the curve changed significantly in the early stage of

imbibition (0.25 d), and the left peak amplitude of the NMR T_2 spectrum curve increased rapidly and shifted slightly to the right, indicating that small-pore imbibition dominated.³² In the middle stage of imbibition (0.25–0.5 days), the amplitude of left and right peaks increased significantly, indicating that small pores and large pores were involved in imbibition, the wetting phase advanced along different pores, and the imbibition rate slowed down. In the late stage of imbibition (0.5–10 days), the left peak amplitude did not change significantly. The wetting phase entered the large pores from the small pores through the diffusion of water molecules, and the imbibition rate slowed and lasted for a long time. When the imbibition is stable, the NMR T_2 spectrum shows a bimodal structure, and the left peak is significantly higher than the right peak, indicating that the main occurrence space of imbibition is small pores, and the smaller pores, the better the imbibition effect. In the process of fracturing fluid imbibition in tight sandstone reservoirs, small pores have a strong capillary force, which has a high contribution rate to imbibition. The imbibition of fracturing fluid first occurs in small pores and then is inhaled by large pores under the diffusion of fracturing fluid so as to carry out imbibition.³³

4. DISCUSSION

4.1. Effect of Physical Properties on Imbibition.

Physical properties characterize the reservoir storage space and seepage space. In the process of spontaneous imbibition, micropores and mesopores are the main imbibition spaces, while macropores, as seepage channels, contribute less to

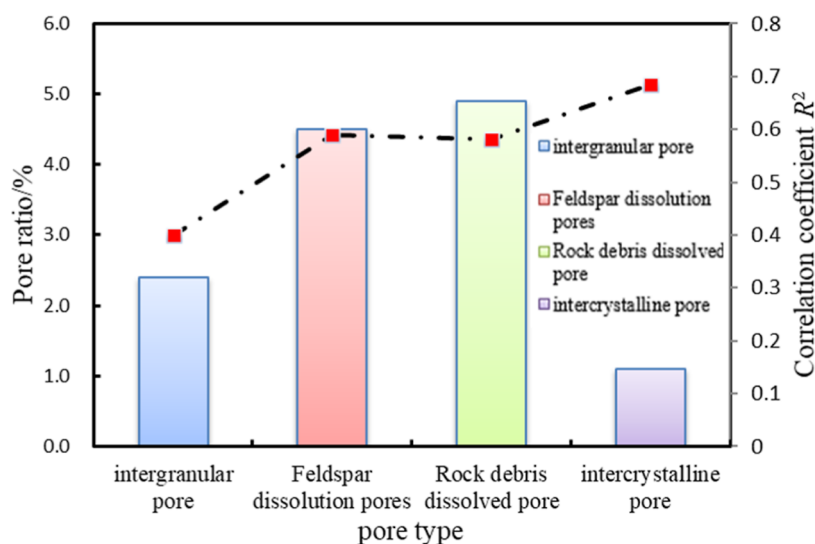


Figure 7. Ratio and correlation of different types of pores.

Table 4. Statistical Table of Pore-Throat Structure Parameters

layer		pore-throat ratio (%)			relative sorting coefficient	pore-throat ratio
		micropore	mesopore	macropore		
He 8	min-value	47.50	24.18	21.97	0.10	136
	max-value	53.85	28.75	25.40	0.34	504
	mean-value	50.31	26.47	23.83	0.24	298

imbibition.³⁴ According to the relationship between porosity, permeability, and imbibition efficiency (Figure 6a), it can be seen that permeability has a high correlation with imbibition efficiency ($R^2 = 0.6422$), that is, permeability has a great influence on reservoir imbibition efficiency. On the whole, combined with the relationship between the imbibition efficiency and the physical properties of the fracturing fluid under different imbibition times in the study area (Figure 6b), it shows a significant positive correlation, indicating that the stronger the reservoir connectivity, the more conducive to the invasion of the wetting phase and the greater the imbibition efficiency. At the same time, with the increase of imbibition time, the correlation coefficient between imbibition efficiency and porosity and permeability is strong and shows a significant increasing trend, indicating that for tight sandstone reservoirs, the better the physical properties, the more conducive to the occurrence of imbibition.

4.2. Effect of the Pore Structure on Imbibition.

4.2.1. Effect of the Pore Type on Imbibition. Affected by the heterogeneity of the reservoir pore-throat structure and throat size, there are significant differences in pore-throat structure characteristics corresponding to different pore types in the study area, and their imbibition efficiency is also very different. The correlation between the proportion of different types of pores and the imbibition efficiency is shown in Figure 7. The correlation between the imbibition efficiency of intercrystalline pores is the highest, followed by dissolution pores, and intergranular pores are the lowest. The reason is that the pore-throat heterogeneity of the intercrystalline pore is weak, and the pore-throat size is small and uniform. In the process of imbibition, the capillary force is strong, and the imbibition efficiency is strongly correlated with the pore ratio, which increases with the increase of the matrix ratio.³⁵ The pore throat heterogeneity of dissolution pores and intergra-

nular pores is strong, which is mainly characterized by a large and uneven throat. In the process of imbibition, the capillary force is not uniform, resulting in a large change in the imbibition efficiency, and the correlation between the imbibition efficiency and pore proportion is weak.

4.2.2. Effect of Aperture on Imbibition. The relative sorting coefficient can accurately reflect the degree of pore connectivity. The smaller the relative sorting coefficient, the better the pore connectivity.³⁶ The relative sorting coefficient parameters obtained from mercury injection are listed in Table 4. The relative sorting coefficient of 6 samples is between 0.1 and 0.34, with an average of 0.24. The influence of the relative sorting coefficient of different samples on imbibition is analyzed, as shown in Figure 8a. The imbibition efficiency decreases with the increase of the relative sorting coefficient, and the correlation coefficient R^2 is relatively large, indicating that the relative sorting coefficient has an obvious influence on imbibition. The uniformity of pore space development can be reflected by the pore-throat ratio. The smaller the pore-throat ratio is, the more uniform the development is. The pore-throat ratio of 6 samples ranged from 136 to 504, with an average of 298. The influence of the pore-throat ratio on the imbibition of different samples was analyzed, as shown in Figure 8b. The imbibition efficiency decreases with an increase of the pore-throat ratio. When the pore-throat ratio is small, the smaller pores are controlled by the larger throat, while the pores with a smaller radius have a larger capillary force, which is conducive to imbibition. Due to the good pore-throat connectivity, the wetting phase can be sucked into the pores smoothly, resulting in higher imbibition efficiency. The correlation coefficient R^2 is relatively small, indicating that the relationship between the pore-throat ratio and imbibition efficiency is weak.

The proportion of different types of pores (Figure 8c) is used to analyze the imbibition efficiency of tight sandstone

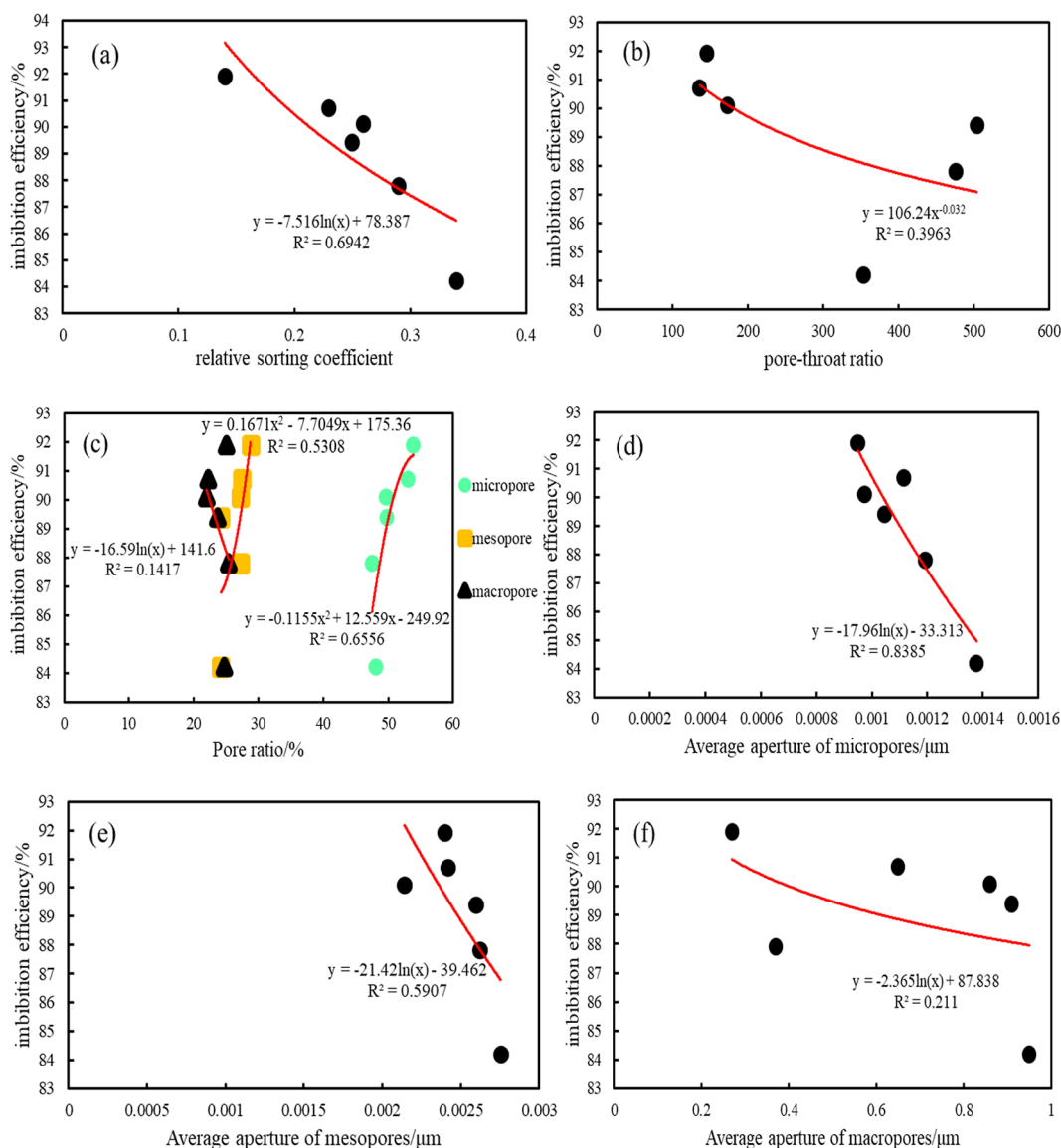


Figure 8. Relationship between pore parameters and imbibition efficiency. (a) Relative sorting coefficient and imbibition efficiency, (b) pore-throat ratio and imbibition efficiency, (c) pore ratio and imbibition efficiency, (d) average aperture and imbibition efficiency of micropores, (e) mesoporous average aperture and imbibition efficiency, and (f) average aperture of macropores and imbibition efficiency.

rock samples. It is not difficult to find that pores of different sizes contribute differently to the imbibition process. The size of various pores has a great influence on the imbibition results. At the same time, the average aperture of various pores (Formula 1) is used to analyze the imbibition efficiency of rock samples in each imbibition period (Figure 8d–f). There are micropores > mesopores > macropores related to imbibition efficiency. The results can well explain the role of capillary force in the process of imbibition. For tight sandstone reservoirs, capillary force is mainly used as imbibition power to develop reservoirs. Small pores produce a large capillary force, which is conducive to imbibition. Macropores have a small capillary force and contribute little to the imbibition efficiency. However, in the case of good pore-throat connectivity, there will be a part of fracturing fluid flowing along the larger pore-throat to the macropores during the imbibition process of small pores, which is conducive to the imbibition of macropores.³⁷

Average aperture calculation formula

$$D = 4 \times \text{adsorption capacity} / \text{specific surface area} \quad (1)$$

4.3. Effect of Fracturing Fluid Performance on Imbibition. The fracturing fluid has different effects on imbibition under different conditions. According to the field water obtained from the field practice in the study area, combined with different fracturing fluid formulations, the imbibition experiments of different fracturing fluids on rock samples were carried out, and the imbibition saturation under different imbibition times was monitored by NMR experiments. The basic parameters of fracturing fluid are shown in Table 5.

4.3.1. Effect of Interfacial Tension on Imbibition. The fracturing fluid with low interfacial tension can effectively reduce the water lock effect, help the fracturing fluid flowback, and protect the reservoir.³⁸ Therefore, it is necessary to study the effect of the interfacial tension of fracturing fluid on imbibition. On the whole (Figure 9a), with the increase of imbibition time, the larger the interfacial tension is, the smaller the imbibition amount is, and the overall variation range of

Table S. Selection of Basic Parameters of the Fracturing Fluid

on-site water	fracturing fluid	interfacial tension (mN/m)	contact angle/deg
0.25% hydroxypropyl guar gum +0.1% bactericide +0.5% short-acting clay stabilizer +0.5% long-acting clay stabilizer +0.3% cleanup agent +0.1% waterproof locking agent +0.01% pH regulator +0.03–0.1% low temperature activator +0.15% accelerated cross-linking agent +0.2% delayed cross-linking agent		1.27	59
0.3% hydroxypropyl guanidine gum +0.1% bactericide +0.5% short-acting clay stabilizer +0.5% long-acting clay stabilizer +0.3% cleanup additive +0.1% waterproof locking agent +0.01% pH regulator +0.02% low temperature activator +0.15% accelerated cross-linking agent +0.2% delayed cross-linking agent		1.32	69
0.3% hydroxypropyl guanidine gum +0.1% bactericide +0.5% short-acting clay stabilizer +0.5% long-acting clay stabilizer +0.3% cleanup additive +0.1% waterproof locking agent +0.01% pH regulator +0.15% accelerated cross-linking agent +0.2% delayed cross-linking agent		1.33	62
0.25% hydroxypropyl guar gum +0.1% bactericide +0.5% short-acting clay stabilizer +0.5% long-acting clay stabilizer +0.3% cleanup agent +0.1% waterproof locking agent regulator +0.02% low temperature activator +0.15% accelerated cross-linking agent +0.2% delayed cross-linking agent		1.36	72
0.3% hydroxypropyl guanidine gum +0.1% bactericide +0.5% short-acting clay stabilizer +0.5% long-acting clay stabilizer +0.3% cleanup additive +0.1% waterproof locking agent +0.01% pH regulator +0.03–0.1% low temperature activator +0.15% accelerated cross-linking agent +0.2% delayed cross-linking agent		1.29	57
0.1% hydroxypropyl guanidine gum +0.1% bactericide +0.5% short-acting clay stabilizer +0.5% long-acting clay stabilizer +0.3% cleanup additive +0.1% waterproof locking agent +0.01% pH regulator +0.1% accelerated cross-linking agent +0.2% delayed cross-linking agent		1.31	65

imbibition efficiency shows a decreasing trend. By analyzing the correlation between imbibition efficiency and interfacial tension (Figure 9b), it can be found that there is a negative correlation between imbibition efficiency and interfacial tension, indicating that the larger the interfacial tension, the smaller the imbibition efficiency is. Low interfacial tension fracturing fluid is more likely to migrate in porous media, and too low or too high interfacial tension will reduce the capillary force,³⁹ which is not conducive to the progress of imbibition. The imbibition efficiency is highest when the interfacial tension is in the range 1.27–1.29 mN·m⁻¹.

4.3.2. Effect of Wettability on Imbibition. For the spontaneous imbibition experiment, during the spontaneous imbibition process of each sample, it can be found that the amount of imbibition gradually decreases with the increase of contact angle at different imbibition times, and the variation range of imbibition efficiency (Figure 10a) gradually decreases. The correlation between different contact angles and imbibition efficiency (Figure 10b) is analyzed. The contact angle is negatively correlated with imbibition efficiency. The stronger the wettability of the rock sample and the fracturing fluid (the smaller the contact angle), the higher the imbibition efficiency. The smaller the contact angle is, the greater the capillary force is, and the capillary force is the main driving force of imbibition. The stronger the capillary force is, the higher the imbibition efficiency is, which is consistent with the law obtained from the above experimental results. Therefore, the wettability of rock samples and fracturing fluid has a non-negligible effect on reservoir imbibition.

4.4. Analysis of Main Controlling Factors and the Imbibition Mechanism. The relationship between the above influencing factors and the absolute value of R² of the imbibition efficiency was used to evaluate the main controlling factors affecting imbibition. It is found that the influence of microscopic factors on the imbibition efficiency is significantly higher than that of macroscopic factors (Figure 11). The correlation degree between each factor and imbibition efficiency is average pore size, interfacial tension, sorting coefficient, intercrystalline pore content, permeability, wettability, and porosity. It can be seen that due to the strong microscopic heterogeneity of tight sandstone, the macroscopic properties cannot directly reflect the microscopic characteristics, and the response relationship to the imbibition efficiency is stronger. The average aperture is the main controlling factor affecting the imbibition, followed by the gas–water interfacial tension. The correlation coefficients between the two and the imbibition efficiency are more than 0.80, reflecting a strong correlation. Therefore, the fine characterization of reservoir aperture and the rapid and accurate determination of gas–water interfacial tension can accurately predict the imbibition efficiency so as to evaluate the possibility of water lock in the formation and the applicability of fracturing fluid selection.

The microscopic mechanism of imbibition was comprehensively analyzed by using nuclear magnetic aperture distribution, full aperture splicing distribution (gas adsorption, mercury intrusion experiment aperture distribution results), nuclear magnetic pseudocolor, contact angle, and scanning electron microscope results (Figure 12). The proportion of imbibition space was determined according to the nuclear magnetic aperture distribution curve before and after imbibition. The intersection point of the nuclear magnetic aperture distribution curve and the full aperture splicing distribution curve determined the mainstream aperture range (the contribution

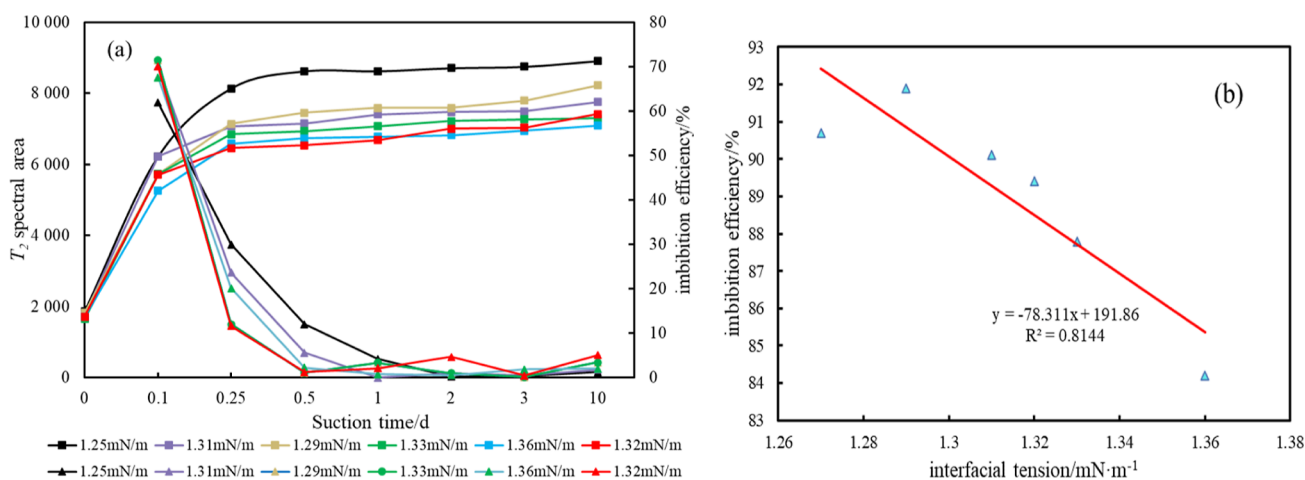


Figure 9. T_2 spectrum area and imbibition efficiency of different interfacial tension fracturing fluids under different imbibition times. (a) T_2 area and imbibition efficiency under different interfacial tensions and (b) correlation between interfacial tension and imbibition efficiency.

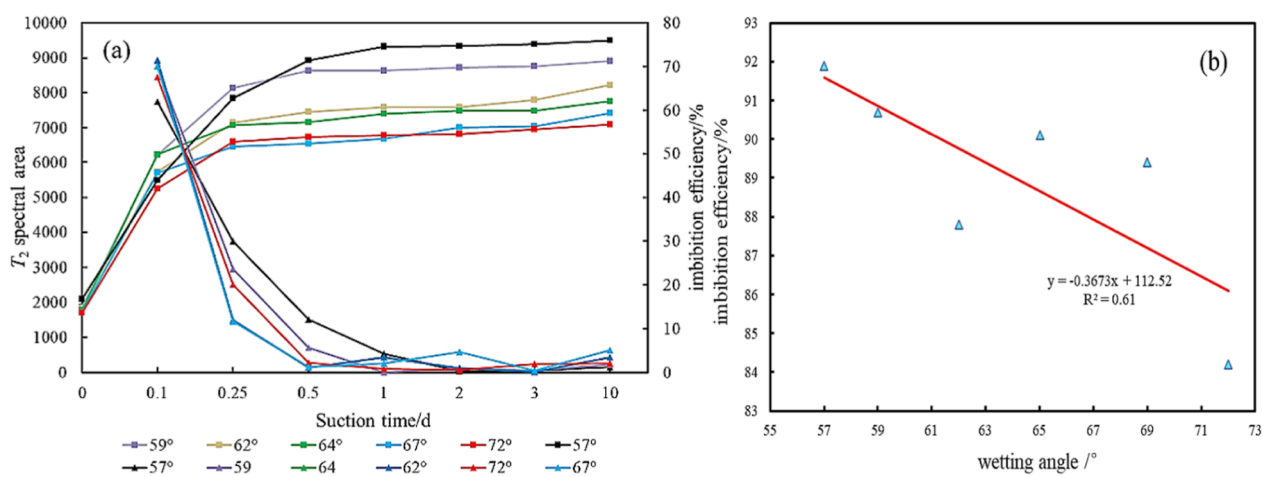


Figure 10. T_2 spectrum area and imbibition efficiency of the fracturing fluid with different contact angles under different imbibition time. (a) T_2 area and imbibition efficiency under different wetting angles. (b) Correlation between the contact angle and imbibition efficiency.

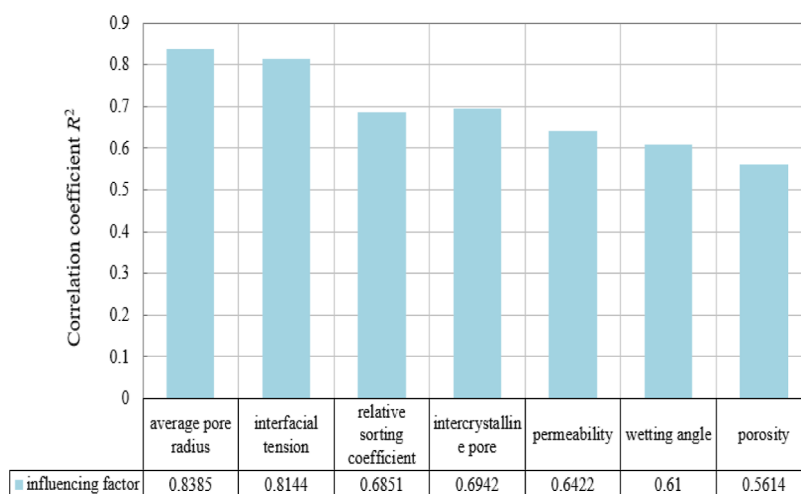


Figure 11. Column analysis diagram of influencing factors.

rate of each aperture was determined by the proportion of fluid signals in micropores, mesopores, and macropores in the mainstream space). The interfacial tension was analyzed by comparing the distribution area of pseudocolor fluid and roundness in the initial stage and stage of imbibition.

Combined with contact angle and electron microscopy, wettability, pore filling, and pore type were analyzed. H1 is selected for comprehensive analysis of rock samples. It can be seen that the infiltration space of the H1 rock sample is 84.25%, the contribution rate of micropores in the mainstream

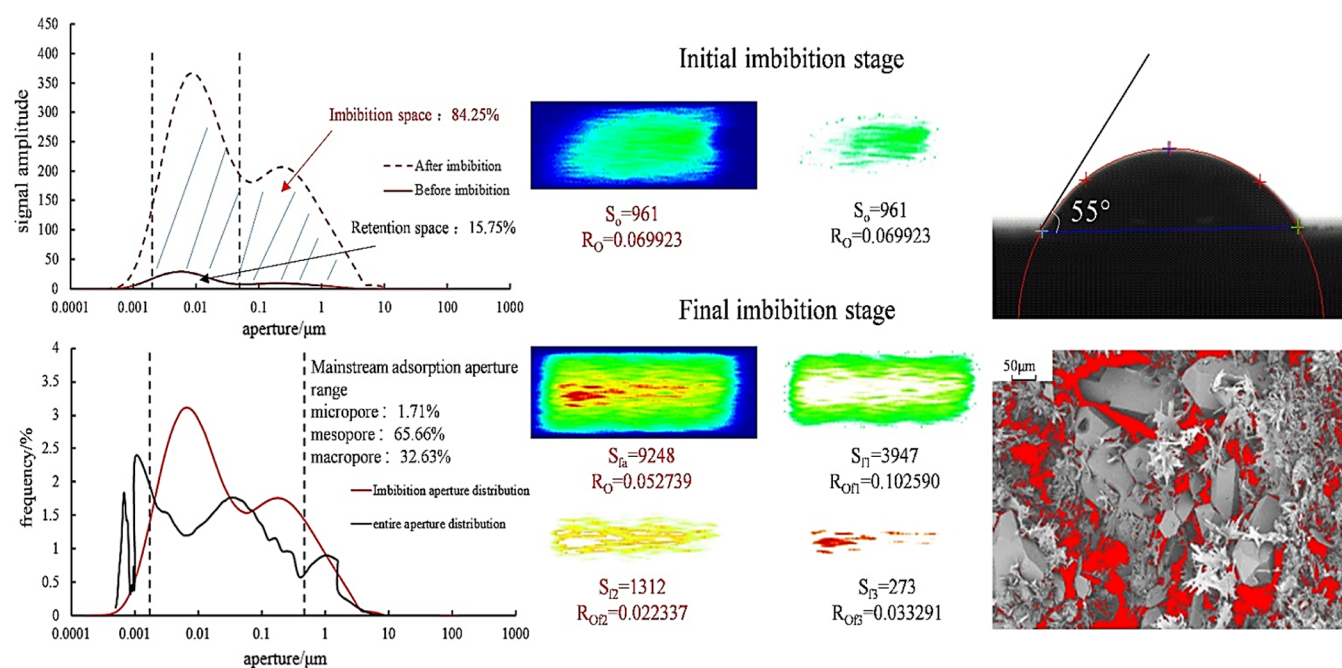


Figure 12. Comprehensive analysis of the microscopic mechanism of imbibition.

aperture space is 1.71%, the contribution rate of mesopores is 65.66%, and the contribution rate of macropores is 32.63%. In the initial stage, the fluid distribution area $S_o = 961$, the average roundness $R_o = 0.069923$, the fluid distribution area $S_o = 9248$, the average roundness $R_o = 0.052739$, and the contact is 55° . According to the factors that affect the imbibition, the aperture has a great influence on the imbibition, and the contribution rate of the micropore and mesopore mainstream aperture space is higher than that of the macropore. The interfacial tension is judged according to the roundness of the nuclear magnetic pseudocolor image. The smaller the roundness, the smaller the interfacial tension. According to the law of roundness change, it can be found that the smaller the interfacial tension, the better the imbibition effect of the fracturing fluid. The relative sorting coefficients reflect the pore connectivity. The smaller the relative sorting coefficient, the better the pore connectivity, which is more conducive to imbibition. The higher the porosity and permeability; the better the imbibition effect, the smaller the contact angle, the better the wettability, and the greater the capillary force, so the smaller the contact angle, the better the imbibition effect. In general, although the smaller the aperture, the higher the imbibition efficiency, the mesopore is the main contribution pore of the imbibition amount, the micropore is the power source of the imbibition, and the mesopore is the main storage space of the imbibition fluid. Since the size of the fracture is generally larger than that of the porous medium, the more complex the fracture, the higher the degree of damage to the water lock. Therefore, in the development of tight gas, from the perspective of working conditions, complex wide fractures should be created to destroy the space where the fracturing fluid may imbibe, thereby inhibiting the water lock and improving the recovery rate.⁴⁰

5. CONCLUSIONS

The small hole provides a strong capillary force to increase the mobility of the fracturing fluid. Therefore, the imbibition efficiency increases with the increase in the small hole.

The pore structure of the He 8 member reservoir in the Linxing area is complex, characterized by nanoscale micropores and throats. Residual intergranular pores, dissolution pores, and intercrystalline pores are the main types of pores. Mercury saturation ranges from 65.36 to 92.90%, generally high, and the presence of large throats and microcracks improves pore connectivity in the region. Significant variations in mercury withdrawal efficiency indicate the substantial impact of reservoir heterogeneity on recovery rates.

The imbibition capacity of tight sandstone reservoirs is less affected by porosity, permeability, and wettability and is mainly controlled by average pore radius, interfacial tension, relative sorting coefficient, and intergranular pore content. The smaller the average pore size and relative sorting coefficient, the higher the imbibition efficiency. There is an optimal range of interfacial tension. Too low or too high of an interfacial tension will reduce the capillary force, which is not conducive to imbibition. The pore throat heterogeneity of intercrystalline pores is weak, and the capillary force is strong, which is conducive to imbibition.

■ ASSOCIATED CONTENT

Data Availability Statement

All data is available within the manuscript.

■ AUTHOR INFORMATION

Corresponding Author

Tian Li – Engineering Research Center of Development and Management for Low to Ultra-Low Permeability Oil & Gas Reservoirs in West China, Ministry of Education, College of Petroleum Engineering, Xi'an Shiyou University, Xi'an 710065, China; Email: dzren@xsyu.edu.cn

Authors

Dazhong Ren – Engineering Research Center of Development and Management for Low to Ultra-Low Permeability Oil & Gas Reservoirs in West China, Ministry of Education, College

of Petroleum Engineering, Xi'an Shiyou University, Xi'an 710065, China; orcid.org/0009-0003-4926-8497

Haipeng Sun – No. 4 Gas Production Plant, Chang Qing Oilfield Company, Petrochina Xi'an Shaanxi, Xi'an 710021, China

Hu Wang – No. 6 Gas Production Plant, Changqing Oilfield Company, PetroChina, Yan'an 716000, China

Tao Tian – Geology Group CO., Ltd. Key Laboratory of Coal Resources Exploration and Comprehensive Utilization, Ministry of Natural Resources, Xi'an 710021, China

Qihui Li – Engineering Research Center of Development and Management for Low to Ultra-Low Permeability Oil & Gas Reservoirs in West China, Ministry of Education, College of Petroleum Engineering, Xi'an Shiyou University, Xi'an 710065, China

Zhen Yan – Engineering Research Center of Development and Management for Low to Ultra-Low Permeability Oil & Gas Reservoirs in West China, Ministry of Education, College of Petroleum Engineering, Xi'an Shiyou University, Xi'an 710065, China

Complete contact information is available at:

<https://pubs.acs.org/10.1021/acsomega.3c10081>

Author Contributions

Conceptualization: T.L. and H.W.; methodology: Z.Y.; software: Q.L.; validation: T.L. and Q.L.; formal analysis: D.R.; investigation: Q.L.; resources: D.R.; data curation: H.S.; writing—original draft preparation: T.L. and Q.L.; writing—review and editing: T.L. and D.R.; visualization— Z.Y.; supervision: H.S.; project administration: T.T.; funding acquisition: T.L. and D.R. All authors have read and agreed to the published version of the manuscript.

Notes

The authors declare no competing financial interest.

ACKNOWLEDGMENTS

The research was sponsored by the National Key R&D Program of China (no. 2023YFE0120700), the Shaanxi Province 2023 Innovation Capability Support Plan (no.2023KJXX-122), Xi'an Shiyou University: Graduate Student Innovation and Practical Ability Cultivation Programme: YCS23213038, and the National Natural Science Foundation of China (no.51934005).

REFERENCES

- (1) Tong, Q.; He, D.; Xia, Z.; Huang, J.; Di, K.; Xu, F.; Guo, S. Influence of Reservoir Pore-Throat Structure Heterogeneity on Water-Flooding Seepage: A Case Study of Yanchang Formation in Ordos Basin. *Minerals* **2022**, *12*, 1243.
- (2) Fu, J. H.; Li, S. X.; Xu, L. M.; Niu, X. B. Paleo-sedimentary environmental restoration and its significance of Chang 7 Member of Triassic Yanchang Formation in Ordos Basin, NW China. *Petrol. Explor. Dev.* **2018**, *45* (6), 998–1008.
- (3) Shi, W. Q.; Cheng, Y. X.; Wu, B.; Yan, L.; Ge, Y. Z.; Chen, M. G. Effect of Surfactants on Imbibition Recovery of Tight Sandstone Reservoirs in Ordos Basin. *Oilfield Chem.* **2023**, *40* (01), 110–116.
- (4) Zhu, W. Y.; Ju, Y.; Zhao, M.; Chen, Q.; Yang, Z. M. Spontaneous Imbibition Mechanism Of Flow Through Porous Media And Waterflooding In Low-Permeability Fractured Sandstone Reservoir. *Acta Petrol. Sin.* **2002**, No. 06, 56–59.
- (5) Wang, Y.; Kang, Y.; Wang, D.; You, L.; Chen, M.; Yan, X. Liquid phase blockage in micro-nano capillary pores of tight condensate reservoirs. *Capillarity* **2022**, *5* (1), 12–22.

- (6) Yang, Z. M.; Liu, X. W.; Li, H. B.; Lei, Q. M.; Luo, Y. T.; Wang, X. Z. Analysis on the influencing factors of imbibition and the effect evaluation of imbibition in tight reservoirs. *Petrol. Explor. Dev.* **2019**, *46* (4), 779–785.

- (7) Liu, X.; Fan, X.; Yin, J.; Zhang, Y. Imbibition Characteristic of Fractured Tight Sandstone Reservoir. *Processes* **2022**, *10*, 2189.

- (8) Xia, Y. X.; Tian, Z. H.; Xu, S.; Wei, W.; Cai, J. C. Effects of microstructural and petrophysical properties on spontaneous imbibition in tight sandstone reservoirs. *J. Nat. Gas Sci. Eng.* **2021**, *96*, 104225.

- (9) Zhou, W. F.; Wang, X.; Lu, X. G.; Pan, H.; Wang, T. T.; Han, D. W. Effects of the dynamic imbibition recovery and its influencing factors for the tight oil reservoirs. *Pet. Geol. Oilfield Dev. Daqing* **2017**, *36* (03), 148–155.

- (10) Cai, J. C.; Li, C. X.; Song, K. P.; Zou, S. M.; Yang, Z. M.; Shen, Y. H.; Meng, Q. B.; Liu, Y. The influence of salinity and mineral components on spontaneous imbibition in tight sandstone. *Fuel* **2020**, *269*, 117087.

- (11) Mirzaei-Paiaman, A.; Kord, S.; Hamidpour, E.; Mohammadzadeh, O. Scaling one- and multi-dimensional co-current spontaneous imbibition processes in fractured reservoirs. *Fuel* **2017**, *196* (May 15), 458–472.

- (12) Chen, J. X.; Yang, Y.; Cao, X. P.; Zhang, S. M.; Lv, Q.; Jiang, L.; Cheng, Z.; Liu, Z. P.; Song, Y.; Li, T. B. Simulation Study on the Spontaneous Imbibition Mechanism and Influencing Factors of Laminated Shale Oil Reservoirs in Jiyang Depression, Eastern China. *Energy Fuels* **2023**, *37*, 13048–13064.

- (13) Gao, H.; Wang, Y. L.; Xie, Y. G.; Ni, J.; Li, T.; Wang, C.; Xue, J. J. Imbibition and Oil Recovery Mechanism of Fracturing Fluids in Tight Sandstone Reservoirs. *ACS Omega* **2021**, *6* (3), 1991–2000.

- (14) Xu, Z. Y.; Cheng, L. S.; Cao, R. Y.; Fang, S. D.; Wu, J. Z.; Zhuang, Y. T.; Ai, S. Characterization of Key Tight Oil Parameters and Mass Transfer of Counter-Current Imbibition in Fractured Tight Oil Reservoirs. *Earth Sci.* **2017**, *42* (8), 1431–1440.

- (15) Zhang, X. P.; Liu, Y. Q.; Liu, Y. Z.; Zhong, C. R. Influencing Factors and Application of Spontaneous Imbibition of Fracturing Fluids in Tight Sandstone Gas Reservoir. *ACS Omega* **2022**, *7*, 38912–38922.

- (16) Busscher, W. Fundamentals of soil behavior. *Soil Sci.* **1994**, *158* (1), 74.

- (17) Wu, Y.; Zhao, Y.; Li, P. Effect of the Heterogeneity on Sorptivity in Sandstones with High and Low Permeability in Water Imbibition Process. *Processes* **2019**, *7*, 260.

- (18) Zaeri, M. R.; Shahverdi, H.; Hashemi, R.; Mohammadi, M. Impact of water saturation and cation concentrations on wettability alteration and oil recovery of carbonate rocks using low-salinity water. *J. Pet. Explor. Prod. Technol.* **2019**, *9* (2), 1185–1196.

- (19) Ren, D. Z.; Liu, D. K.; Zhou, Z. H.; Zhou, R.; Liu, N.; Sun, W. Research on waterflooding efficiency of tight sandstone reservoir and its microscopic influence factors: Taking the Triassic chang 6 member in Huaqing area, Ordos basin, NW China as an example. *J. Chin. Electron Microsc. Soc.* **2019**, *38* (04), 364–375.

- (20) Liu, D.-K.; Sun, W.; Ren, D.-Z.; Zhang, Q.; Ming, H.-X.; Chen, B. Features of pore-throat structures and movable fluid in tight gas reservoir: A case from the 8-(th) member of Permian Shanxi Formation in the western area of Sulige Gasfield, Ordos Basin. *Nat. Gas Geosci.* **2016**, *27* (12), 2136–2146.

- (21) GB/T2150.1–2008. Determination of aperture distribution and porosity of solid materials by mercury intrusion porosimetry and gas adsorption part 1: mercury intrusion porosimetry. S.

- (22) Li, C.; Liu, X.; You, F.; Wang, P.; Feng, X.; Hu, Z. Pore Size Distribution Characterization by Joint Interpretation of MICP and NMR: A Case Study of Chang 7 Tight Sandstone in the Ordos Basin. *Processes* **2022**, *10*, 1941.

- (23) Yang, X.; Liao, R. Q.; Yuan, X. Spontaneous imbibition experiment in high-temperature and high-pressure for tight cores based on NMR technology. *Pet. Geol. Oilfield Dev. Daqing* **2023**, *42* (03), 58–65.

(24) GB/T21650.2–2008. Determination of aperture distribution and porosity of solid materials by mercury intrusion method and gas adsorption method part 2: analysis of mesopores and macropores by gas adsorption method. S.

(25) SY/T 6490–2014. Laboratory measurement specification of nuclear magnetic resonance parameters of rock samples. S.

(26) Yao, L. L.; Yang, Z. M.; Li, H. B.; Cai, B.; He, C. M.; Xia, D. B. Study on mechanism of spontaneous imbibition and pressurized imbibition in shale oil reservoirs. *J. Pet. Explor. Prod.* **2021**, *11* (2), 703–710.

(27) Zhou, Y.; Li, S.; Bai, Y.; Long, H.; Cai, Y.; Zhang, J. Joint Characterization and Fractal Laws of Pore Structure in Low-Rank Coal. *Sustainability* **2023**, *15*, 9599.

(28) Xu, S.; Yang, Z.; Wu, S.; Wang, L.; Wei, W.; Yang, F.; Cai, J. C. Fractal Analysis of Pore Structure Differences Between Shale and Sandstone Based on the Nitrogen Adsorption Method. *Nat. Resour. Res.* **2022**, *31*, 1759–1773.

(29) Li, T.; Ren, D. Z.; Ning, B.; Li, Q. H.; Zhang, H. P.; Zhou, J. L.; Zhang, Z. F. Multi-scale joint characterization of coal seam pore structure and its influence on movable fluid. *J. Min. Sci. Technol.* **2023**, *8* (04), 569–582.

(30) Dong, J.; Huang, Z.; Chen, J.; Li, T.; Zhao, J.; Pan, Y.; Qu, T. Pore Structure and Fractal Characteristics of Tight Sandstone: A Case Study for Huagang Formation in the Xihu Sag, East China Sea Basin, China. *Energies* **2023**, *16*, 2013.

(31) Thommes, M. Physisorption of gases, with special reference to the evaluation of surface area and pore size distribution (IUPAC Technical Report). *Pure Appl. Chem.* **2016**, *38* (1), 25.

(32) Yang, X.; Liao, R. Q.; Yuan, X. Spontaneous imbibition experiment in high-temperature and high-pressure for tight cores based on NMR technology. *Pet. Geol. Oilfield Dev. Daqing* **2023**, *42* (03), 58–65.

(33) Zhou, X. H.; Chen, D. X.; Xia, Y. X.; Zeng, J. H.; Qiao, J. C.; Xu, X.; Cai, J. C. Spontaneous Imbibition Characteristics and Influencing Factors of Chang 7 Shale Oil Reservoirs in Longdong Area, Ordos Basin. *Earth Sci.* **2022**, *47* (8), 3045–3055.

(34) Ren, W. D.; Ma, C.; Huang, X. Y.; Gu, W.; Chen, Y.; Liu, X. Y. Dynamic and static imbibition characteristics of tight sandstone based on NMR. *Geoenery Sci. Eng.* **2023**, *229*, 212052.

(35) Li, M.; Liao, J.; Wang, S.; He, Z. X.; Wang, H. W.; Wang, J.; He, H.; Zhu, Y. S. Imbibition characteristics and influencing factors of reservoirs with ultra-low permeability of Ordos Basin: a case study of third member of Triassic Yanchang Formation in Weibei Oil Field. *Pet. Geol. Exp.* **2022**, *44* (06), 971–980.

(36) Jia, X. M.; Lin, Y. B.; Chen, L.; Zhang, H. Study on difference of pore structure in macroscopic coal rock composition based on mercury intrusion method. *Saf. Coal Mine* **2022**, *53* (06), 19–25.

(37) Wang, C.; Gao, H.; Gao, Y.; Fan, H. M. Influence of Pressure on Spontaneous Imbibition in Tight Sandstone Reservoirs. *Energy Fuels* **2020**, *34* (8), 9275–9282.

(38) He, D. X. Research and application of re-fracturing with imbibition technology in low permeability and tight oil reservoir. *Chem. Eng. Oil Gas* **2023**, *52* (02), 99–103.

(39) Yang, K.; Wang, F. Y.; Zhao, J. Y. Experimental study of surfactant-enhanced spontaneous imbibition in fractured tight sandstone reservoirs: The effect of fracture distribution. *Pet. Sci.* **2023**, *20* (1), 370–381.

(40) Zhu, C. F.; Guo, W.; Wang, Y. P.; Li, Y. J.; Gong, H. J.; Xu, L.; Dong, M. Z. Experimental study of enhanced oil recovery by CO₂ huff-n-puff in shales and tight sandstones with fractures. *Pet. Sci.* **2020**, *18* (3), 852–869.